第 48 卷 第 8 期
2021 年 8 月

湖南大学学报（自然科学版）
Journal of Hunan University（Natural Sciences）

Vol. 48. No. 8.
August 2021

Open Access Article

# COVID-19 Recognition Using Self-Supervised Learning Approach in Three New Computed Tomography Databases

**Amgad Muneer[1], Rao Faizan Ali[1], Suliman Mohamed Fati[2], Sheraz Naseer[3]**

[1] Department of Computer and Information Sciences, Universiti Teknologi PETRONAS, Perak, Malaysia

[2] College of Computer and Information Sciences, Prince Sultan University, Riyadh, Saudi Arabia

[3] Department of Computer Science, University of Management and Technology, Lahore, Pakistan

**Abstract:** Pretraining has been a widely used approach in computer vision and natural language processing, as it typically results in significant performance improvements. The most commonly used pretraining method is transfer learning (TL), which uses labeled data to develop a suitable representation network. Recently, a novel technique for pretraining, self-supervised learning (SSL), has shown promise in various applications. Computed Tomography (CT) is a convenient way to diagnose COVID-19 patients during the COVID-19 pandemic phase. However, openly accessible COVID-19 datasets are highly problematic to gain, which hampers the investigation, and the growth of AI-powered diagnosis approaches of COVID-19 depending on CTs. By using an open-source dataset COVID-CT solve this problem, comprising of 349 COVID-19 CT images. This paper uses three CT datasets to introduce a diagnostic approach based on contrastive self-supervised learning (CSSL) and TL. The effectiveness of CSSL demonstrates an improvement in learning representations. Using multi-task learning and leveraging CSSL pretraining by incorporating lung masks and lesion masks, the authors achieved an accuracy of 0.89 with an F1 of 0.90 and AUC of 0.98.

**Keywords:** transfer learning, self-supervised learning, COVID-19, computed tomography, lung mask, lesion mask.

## 在三個新的計算機斷層掃描數據庫中使用自我監督學習方法識別 新冠肺炎

**摘要:** 預訓練一直是計算機視覺和自然語言處理中廣泛使用的方法，因為它通常會顯著提高性能。最初，最常用的預訓練方法是遷移學習 ，它涉及使用標記數據來開發合適的表示網絡。最近，一種用於預訓練、自監督學習 的新技術在各種應用中顯示出前景。計算機斷層掃描 是在 新冠肺炎 大流行階段診斷 新冠肺炎 患者的便捷方法。然而，可公開訪問的 新冠肺炎 數據集很難獲得，這阻礙了調查，以及依賴 計算機斷層掃描 的人工智能驅動的 新冠肺炎 診斷方法的發展。通過使用包含 349 張 新冠肺炎計算機斷層掃描 新冠肺炎 計算機斷層掃描 解決了這個問題。本文介紹了一種基於對比自監督學習 和使用三個 計算機斷層掃描 數據集的 遷移學習的診斷方法。 對比自監督學習 的有效性證明了學習表示的改進。使用多任務學習並通過結合肺面具和病變面具利用 對比自監督學習 預訓練，我們達到了 0.89 的準確度，F1 為 0.90，AUC 為 0.98.

**關鍵詞**： 轉移學習，自我監督學習，新冠肺炎，計算機斷層掃描，肺面罩，病變面罩。

## 1. Introduction

As of Jun. 03, 2020, COVID disease, a contagious infection that triggered about 386,000 deaths worldwide, out of 6.5 million affected people, lack of testing is one of the core challenges in handling this infection's transmission. Currently, Reverse Transcription Polymerase Chain Reaction (RT-PCR) is the method that is used in testing. However, RT-PCR test kits were short at peak time. Furthermore, numerous suspicious cases continued to transmit the infection to others unknowingly, as they could not be tested timely. Therefore, health facilities have used

Received: May 1, 2021 / Revised: June 6, 2021 / Accepted: July 8, 2021 / Published: August 30, 2021

About the authors: Amgad Muneer, Rao Faizan Ali, Department of Computer and Information Sciences, Universiti Teknologi PETRONAS, Perak, Malaysia; Suliman Mohamed Fati, College of Computer and Information Sciences, Prince Sultan University, Riyadh, Saudi Arabia; Sheraz Naseer, Department of Computer Science, University of Management and Technology, Lahore, Pakistan

alternate diagnosis approaches to reduce the scarcity of RT-PCR test kits. CT scans are used for screening and diagnosing COVID-19, amongst them.

For instance, CT and other imaging procedures are terms as practical techniques for identifying SRAS-COV-2. In Diagnosing and Treatment Protocol of COVID (Trial Version 5) developed in National Health Commission and State Administration Traditional Chinese Medicine in China. To diagnose COVID-19, Numerous health facilities in China use CT scans according to this recommendation, which has been reliable. A professional radiologist diagnosed and treated COVID patients since the beginning of this pandemic in Tongji Hospital, Wuhan, China, was consulted to analyze better CTs' effect in diagnosing COVID. As per the findings of this radiologist, CT helps diagnose COVID-19 during the outbreak period, but CT may not be useful outside of the outbreak period.

Following are the reasons: It is possible to use CT to determine if a person is infected with viral pneumonia or not (COVID-19 virus induces COVID-19 that is a sort of viral pneumonia). Nevertheless, CT cannot tell which virus is triggering viral pneumonia: COVID-19 or others. Therefore, it would be legally correct to say that CTs should not confirm if COVID-19 contaminates the person. Nonetheless, in this pandemic, COVID-19 caused various Viral pneumonia. As per CT findings, a person affected with viral pneumonia is most probably be involved with COVID-19. Keeping this fact in consideration, in this pandemic, CTs are found beneficial in diagnosing COVID-19.

Radiologists are extremely busy during the COVID-19 outbreak and could not promptly go through a range of CT scans. Moreover, as this infection is comparatively new, the radiologists may not be well qualified to identify COVID-19 from CT scans in underdeveloped areas like countryside regions. Numerous papers like 2020 [1, 2] established detailed learning approaches to monitor CTs of COVID-19. However, the CT scans used in these studies are not openly shared because of secrecy issues. Depending on this fact, the investigations and expansions of a more progressive AI approach for additional precise CT-based screening of COVID-19 are critically hampered.

We created COVID-19 CT data sets to overcome this matter, containing 349 COVID-19 positive image data of 216 individual cases and 397 COVID-19 negative CT image data cases. The stated CT imageries were extracted, and those comprising COVID-19 clinical findings were physically selected from 760 medRxiv preprints and bioRxiv preprints about COVID-19 by analyzing the descriptions of these imageries. Numerous responses stating apprehensions related to this dataset's practicality were received after the release of this dataset. The following summary of the core concerns: The quality of images of the real CT is compromised then put in the papers, which can cause issues in the diagnosis decision's accuracy. Losing the Hounsfield Unit (HU) value, reducing the number of bits per pixel, and reducing the image resolution are the quality degradations. In addition, when putting it on paper, only a few key slices are selected from a sequence of CT slices that combine to form an original CT scan, affecting the overall diagnosis.

Concerning these issues, the authors approached the radiologist mentioned above at Tongji Hospital in China. The accuracy of the diagnostic decisions does not get affected significantly, as per the radiologist's opinion. Low-quality CT images do not affect the diagnosis of a skilled radiologist. For instance, a qualified radiologist can make a precise diagnosis by looking at the images taken from the low-resolution camera (mobile camera) of original CT images, even though the quality is compromised. Similarly, the diagnosis's precision is not compromised by the difference in qualities of the CT printed images and the original images. The CT scan image's single slice has sufficient clinical data in precise decision-making even though analyzing a complete CT slices sequence.

CT images from papers are obtained for model exercise only, not for assessment [18]. Real images bestowed by the Clinical facilities are used for training and testing. Real CT images are used to conduct validation. The model trained extracted from paper CT images and the model trained on the real CT images are compared, and the prior surpasses the latter. The CT images of COVID-19 mined from the literature are proved to be beneficial for the diagnosis models of COVID-19. Conclusively, to train the COVID-19 diagnosis model grounded on multi-task learning and self-supervised learning, CT's real images were obtained somewhere else, the lesion marks categorized by the radiologists. This model attains 0.90 F1, 0.98 AUC, and 0.89 accuracy. Models with these kinds of results are great enough for clinical use, as per the skilled radiologist.

Following are the core contributions of this article: (1) The CT images of 349 positive COVID-19 out of 216 patients are collected that combines to form the datasets of COVID-19. (2) In developing COVID-19 diagnostic models by trial studies, this data set's practicality is proved. (3) To increase clinical precision, the authors have established approaches focused on multi-task learning and contrastive self-supervised learning.

## 2. Related Work

There have been many efforts to use deep learning methods to screen COVID-19 from medical images such as CT and chest X-rays. Wu et al. developed an early screening classifier based on multiple CNN models to identify the CT scans of patients diagnosed with COVID-19 [3]. Afterward, some papers propose a 3D deep CNN method, which used chest CT slices to

detect the COVID-19 [4]. Some authors use CNN as a useful research tool to identify the patent number of patients based on the chest X-ray images. Using 3D deep learning, several researchers use this model to screen the chest CT images of COVID-19 [2, 5].

Yang et al. developed a system that is based on deep learning to diagnose DeepPneumonia. This model help health professional to identify patient with COVID-19 [6]. Shen et al. [7] proposed an infection-size-aware Random Forest (iSARF) method, automatically organizing subjects into groups using different infected lesion sizes. Unfortunately, most of the studies do not have the data published publicly.

Due to potential privacy concerns and information blockade, few sufficient datasets with medical images on COVID-19 are available to the public [8]. The existing datasets on COVID-19 are mainly X-ray images [8, 9].

The Italian-based society named SIRM provides chest X-rays and CT images of 68 patients. Moore et al. collected the axial and coronal CTs from the 59 patients and released them at Radiopedia. Data from other sources provide medical images of no more than ten patients.

## 3. COVID-19 CT Dataset

The building process of the dataset of COVID-19 is stated in this section. From Jan. 19 to Mar. 25, the 760 preprints about COVID-19 from medRxiv and bioRxiv were gathered. Most of these preprints mention COVID-19 patients reports, and a few of them present CTs in the papers. CT images are also related to titles in the CT images explaining the clinical changes. To collect the low-level structure material of the preprint PDF, PyMuPDF is used, and AI, the encoded figures are found. Well, preserving the quality of the figures, including the resolution and size, etc. The titles linked with the figures were also recognized from the structure material info.

The CT images are manually selected, provided by these extracted figures and titles. The related image title for every image is read to analyze whether it is COVID-19 positive. If it is impossible to explore from the title, text analyzing the figure in the preprint works to make the final verdict. Metadata including age, gender, location, medical history scan time, intensity, and radiology report were also gathered from each CT image paper.

In the end, 349 CT images titled COVID-19 positive were gathered. The CT images vary according to their sizes. For example, 153 is the minimum height, 491 is the average height, and 1853 is the maximum height. Similarly, 124, 383, and 1485 are the minimum, average, and maximum width. These image data come from 216 patients. We can see some cases of COVID-19 CT images in Figure 1.

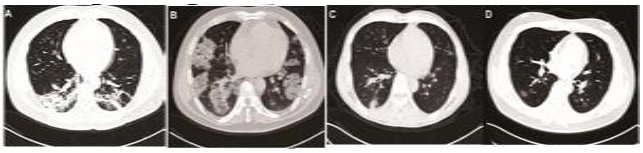

Fig. 1 CT images on admission to hospital of patients infected with SARS-COV-2. A) Chest CT scan from a 39-year-old man with bilateral ground-glass opacities; B) Chest scan from a 45-year-old man with bilateral ground-glass opacities; C) Chest CT scan from a 48-year-old man who was discharged after nine days shows patchy shadows, and D) Chest CT scan from a 34-year-old man who was discharged after 11 days shows patchy shadows

Among the patients titled as positive, 137 display gender data and 169 display age data. The age distribution of COVID-19 patients is shown in Figure 2.

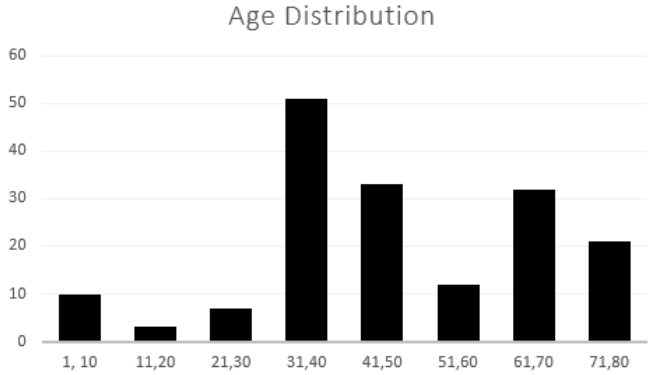


Fig. 2 Data sets of COVID-19 are compared to others in Table 1

Table 1 Comparison of COVID-19 CT Datasets

| Dataset | Images | Patients | Open-Source | Metadata |
|---|---|---|---|---|
| COVID-CT | 349 | 216 | Yes | Yes |
| COVID-19 Images Data Collection [8] | 84 | 45 | Yes | Yes |
| SIRM COVID-19 Database | 100 | 60 | Yes | Yes |
| COVID-CS [10] | 68626 | 400 | No | No |
| COVID-19 CT Segmentation Dataset [20] | 379 | 20 | Yes | No |

Other than COVID-19 image data collection and the SIRM COVID-19 database, the authors' data set has more COVID-19 positive images and patients. COVID-19 CS is not for public access. There are few patients but more COVID-19 positive imageries in the COVID-19 CT segmentation data set. Visually the CT scan images of the same affected person are extremely alike. Consequently, the variety of images in the authors' dataset is greater than those in the COVID-19 CT segmented data set.

To establish binary classification models for diagnosing COVID-19, Non-COVID-19 CT images as negative test examples are gathered. Additionally, concerning the 349 COVID-19 CT images, the set of

Non-COVID-19 CT images as negative test samples is also collected.

These images' source includes the following:

- The MedPix database comprises more than 9,000 subjects, 59,000 imageries, and 12,000 patients and is an open-source online database of medical images, teaching cases, and clinical topics.
- The LUNA dataset: Consists of CT scans images of 888 lung cancer patients.
- The Radiopaedia website: Comprises 36559 patient's radiology images.
- The PubMed Central (PMC): A free full-text collection of journal literature for biomedical and life sciences.

For trained models' evaluations, a test set and validation image set are collected. All imageries are real CT scans collected from hospitals in these two data sets. Not any of them is obtained from papers. The initial COVID-19, including 20 axial volumetric scans, originate from the COVID-19 CT segmentation data set (COVID-Seg) [21]. LUNA and Radiopedia provide the Non-COVID-19 CT images. The composition of the test sets can be seen in Table 2.

Table 2 Statistics of the test set

| No | Class | LUNA | COVID-SEG | RADIO-PEDIA | Total |
|---|---|---|---|---|---|
| No. of Patients | COVID | 0 | 4 | 0 | 4 |
| | Non-COVID | 19 | 0 | 1 | 20 |
| No. of Images | COVID | 0 | 173 | 0 | 173 |
| | Non-COVID | 164 | 0 | 4 | 168 |

From the total of 4 patients, the 173 COVID-19 CT images come in the COVID-Seg data set. Total 168 CT images are included from negative COVID-19: Out of which 164 are in LUNA Data set from 19 patients and remaining are from 1 individual in Radiopedia. The validation set's composition has been shown in Table 3.

From 4 patients in COVID-SEG, CT images of 88 COVID-19 are included. It comprises CT images from 64 negative COVID-19: 48 are from 38 patients.

Table 3 Statistics of the validation set

| No | Class | LUNA | COVID-SEG | RADIO-PEDIA | Total |
|---|---|---|---|---|---|
| No. of Patients | COVID | 0 | 4 | 0 | 4 |
| | Non-COVID | 38 | 0 | 1 | 39 |
| No. of Images | COVID | 0 | 88 | 0 | 88 |
| | Non-COVID | 48 | 0 | 16 | 64 |

LUNA Data set, and the remaining 16 are from 1 individual in Radiopedia. Luna images are sometimes normal and sometimes about lung cancer. The Radiopedia images are regular images. Using the threshold segments and convex hull detection approaches, the chest portion is cropped automatically in images and eliminates extra areas. The statistical of the negative data are shown in Table 4.

Table 4 Statistics of negative data

| No | Class | LUNA | COVID-SEG | RADIO-PEDIA | Total |
|---|---|---|---|---|---|
| No. of Patients | COVID | 17 | 55 | 2 | 72 |
| | Non-COVID | 36 | 195 | 30 | 261 |

# 4. Methodology

The authors conduct experimental research in this study to determine if the pictures in COVID-CT are suitable for training CT-based diagnostic models. The authors end by comparing experimental conditions to three distinct positive training datasets.

*COVID-Seg:* 118 positive CTs in COVID-Seg are taken as positive training examples where CT images archive from datasets.

*COVID-CT-349:* The full set of 349 COVID-19 CTs in COVID-CT-349 are used as positive training examples. The following images are taken out from papers.

*COVID-CT-118:* Randomly taken samples, which are exactly 118 images from COVID-CT, act as positive training samples; this is taken out from papers.

Test images, validation images, and negative training images are the same for the three settings mentioned earlier, as shown in Tables 2, 3, and 4. From the image archiving systems in hospitals, original CT images and images used for validation are extracted. To classify a CT image as COVID-19 or non-COVID-19 DenseNet-169 [10] and ResNet-50 [11] models are used. ImageNet [12] dataset models have already been trained. Three metrics are used to evaluate these trained models: accuracy, F1, and area under ROC curve (AUC). From the image archiving in datasets, original CT images and images used for validation are extracted. To classify a CT image as COVID-19 or non-COVID-19, DenseNet-169 [10] and ResNet-50 [11] models are used. Three metrics are used to evaluate these trained models: accuracy, F1, and area under ROC curve (AUC).

The CT images are manually selected, provided by these extracted figures and titles. The related image title for every image is read to analyze whether it is COVID-19 positive. If it is impossible to analyze from the title, text analyzing the figure in the preprint works to make the final verdict. Metadata including age, gender, location, medical history scan time, intensity, and radiology report were also gathered from each CT image paper.

In the end, 349 CT images titled COVID-19 positive were gathered. The CT images vary according to their sizes. 153 is the minimum height, 491 is the average height, and 1853 is the maximum height. Similarly, 124, 383, and 1485 are the minimum,

average, and maximum width. These image data come from 216 patients. We can see some cases of COVID-19 CT images in Figure 1.

### 4.1. Experimental Settings

Images that are inserted are resized to a vertical resolution of 480-by-480. Then performed data augmentation on the training set. All training images are amplified with random cropping to an exact scale of 0.5, random contrast, horizontal IP, and brightness(random) with a factor of 0.2. Weight parameters available in networks are developed using Adam [13] with a 0.0001 initial learning rate, and the mini-batch size was 16. Cosine Scheduling is set with a period of 10 to maintain the learning rate throughout the training process. PyTorch is used to implement the network.

Three settings of positive training images are shown in the results of Table 4 on the test set. From this table, the authors note: First, the model trained on COVID-CT- 349 is massively improvised/better than trained on COVID-Seg. Images extracted from papers contain COVID-CT-349. COVID-Seg contains original CT images. It shows that COVID-CT is considered useful for training CT-based diagnosis models for the virus COVID-19. Images that are extracted from papers are usually low-quality and single slices. Second, the model trained on COVID-CT-118 is not better than the COVID-CT-349. Adding more COVID-CT images to the training set improves performance considerably, showing how the CTs in COVID-CT have high benefits in training COVID-19 diagnosis models. Third, COVID-CT_118 is outperformed by COVID-Seg. These sets have the relatively same amount of images present. This proves that an original CT is more helpful for model training than a CT obtained from papers on an average scale. Paper extracted CTs are easy to be achieved than original CTs. These results prove the usefulness of the authors' COVID-CT dataset in training diagnosis models of COVID-19.

### 4.2. Experimental Results

First, the model trained on COVID-CT-349 is much enhanced/better than the model trained on COVID-Seg. COVID-CT-349 is present in images extracted from papers. COVID-Seg contains original computed tomography (CT) images. It demonstrates the utility of COVID-CT in training CT-based diagnostic models for the virus COVID-19. Typically, images taken from publications are of low quality and consist of single slices. Second, the model trained on COVID-CT-118 does not perform better than the model trained on COVID-CT-349.

Adding more COVID-CT pictures to the training set significantly increases performance, demonstrating once again how the CTs in COVID-CT are extremely beneficial for training COVID-19 diagnostic models. Third, COVID-CT 118 performs better than COVID-Seg. These collections include a similar number of photos. This demonstrates that an original CT is more beneficial for model training than an average-scale CT obtained from papers. In any case, paper-extracted CTs are more straightforward to get than original CTs. Additionally, these results demonstrate the use of the authors' COVID-CT dataset for developing COVID-19 diagnostic algorithms.

Table 5 Performance of test sets by using DenseNet-169 and ResNet-50

| Model | Positive Training Data | Accuracy % | F1-score % | AUC % |
|---|---|---|---|---|
| DenseNet-169 | COVID-Seg | 69.8 | 61.1 | 86.9 |
| | COVID-CT-349 | 79.5 | 76.0 | 90.1 |
| | COVID-CT-118 | 57.8 | 36.3 | 75.2 |
| ResNet-50 | COVID-Seg | 66.3 | 58.1 | 80.6 |
| | COVID-CT-349 | 77.4 | 74.6 | 86.4 |
| | COVID-CT-118 | 60.4 | 42.6 | 74.1 |

## 5. Improving Model

There is a total of 467 positive images in COVID-CT and COVID-SEG. On such a limited number of images, the training deep learning models are vulnerable to errors. Two approaches are used to study this issue: Counting the lung region's segmentation masks and lesion region's segmentation masks by combining additional information or learning healthier visual representation. Rather than paying close consideration to the unrelated areas to COVID-19, lung mask advises models to start paying extra consideration to lung regions that include COVID-19 clinical manifestations. The images have a noticeably grainy appearance as the search space of COVID-19 is narrowed down by the lung mask. The minimal area is acquired by the regions affected with COVID-19 in the lung's region.

Lesion masks can classify areas that need special attention, and it gives fine-grained guidance to the model. Lesion masks are much harder to get as they have a higher accuracy rate. Unlike lungs masks, these titles can be delivered only by the skilled radiologist, which any non-medical person can title. The lungs can title the COVID-CT and COVID-SEG test images, negative or positive. Lesion mask individually titles COVID-SEG positive images. According to this evidence stated, Diverse approaches are used to apply lesion masks and lung masks. On the input end of the diagnostic model, lung masks are integrated.

A lung segmentation model is established, founded on the residual U-Net [14], utilizing the lungs masks in COVID-CT and COVID-SEG. During training or testation, the segmentation models are utilized to detect the lung masks using a CT image, linking it with the CT images, and put them into the diagnostic model, as shown in Figure 3A. Information of the lung segmentation trials is delayed with the supplements, as shown in Figure 3B. At the same time, testing models,

at the output of the diagnostic model, the Lesion masks are combined. This administrates the models to give improved consideration to the areas comprising the lesions.

Instantaneously, for joining the lesion masks and the lung masks, the construction can be seen in Figure 3C when the sum of characterization loss and lesion segmentation loss is minimized. Simultaneously, testation, the class title, and lesion masks are predicted by the CT image (Even if it is a COVID-19 positive or negative image). The lungs segmentation model is used provided by CT image to get lungs to mask. Along with the lungs mask image, the real CT image is processed in series and put into the network that extracts features.

The graphic features are loaded into ASPP (Atrous Spatial Pyramid Pooling) sheet [15] to obtain a dense and high-resolution feature map. Two branches extract from these structure maps:

- Lesion Segmentation Branch: To predict Lesion Segmentation Mask.
- Classification Branch: To predict the class title.

As an extra intelligence, the classification branch gets the foretold lesion segmentation mask. In between the ground truth mask and foretold mask, a classification loss is established. To identify the weight parameters for knowledge in the system, the addition of the two losses is reduced. It is to be noticed that the Lesion masks are only desired during the period of training. The estimate is made throughout the testing depending on the test images and the lung segmentation masks. The Lesion Mask is not needed. Figure 3 shows the proposed transfer learning approach used in this study to recognize COVID-19 from patients' CT scans.

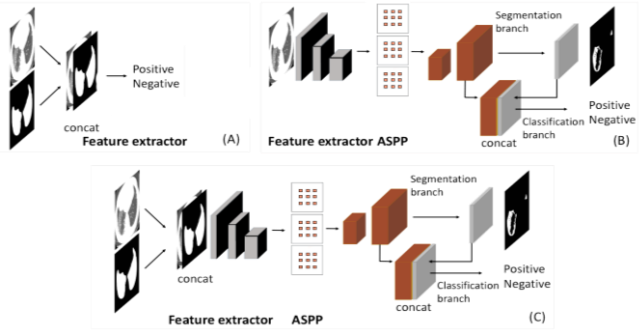


Fig. 3 Detecting COVID-19 from CT Scan Datasets using the proposed transfer learning approach

There are supplementary methods to advance the presentation [16]. Utilizing the transfer learning, on ImageNet, the weights in Dense Net 169 and ResNet-50 are pre-trained. At the time of training, in Image Net, the class titles are grasped. Models might be prejudiced to universal domain classes and generalize less well on sorting COVID-19, pre-trained by Image Net, as Image Net classes are usually non-medical. In COVID-19 diagnosis, on testing CT images, Contrastive Self Supervised Learning (CSSL) is used to perfect the Image Net pre-trained models to prevent this racism. CSSL is an unsupported method. By resolving a supplementary mission, it acquires representation. CSSL develops augmented CT samples, then by resolving the estimation issue, the graphical representation network studies if both the augmentations come out of the same C or not. No titles are used. Only the input CT image is used at the time of training. The network is more tuned up through the input CT images and the output titles once done with the training.

### 5.1. Experiments on an Improved Model

As per experimental settings in a multi-task learning framework, the weights linked to segmentation loss and classification loss are assigned 1. The remaining hyperparameter settings are similar to the settings of Section 3. We adopt the identical hyperparameter setting for comparing self-supervised learning as in MoCo [7]. Augmentation with an arbitrary horizontal flip is done for every single input image, an arbitrary value of size 0.2 to crop area in the image, random color twitching, *i.e.*, 0.4 ratios of arbitrary brightness, 0.4 arbitrary contrast, 0.4 saturation, 0.1 arbitrary hues, arbitrary greyscale alteration, and Gaussian blur. 512 is the value size for a dynamic dictionary as the optimizer with the 128 sizes of minibatch, 0.0001 of decay weight, 0.9 momenta, and 0.015 of starting learning rate, stochastic gradient descent (SGD) has been utilized [17].

On training data, the working of Dense Net 169 is shown in Table 6. The joint test data set of COVID-349 and COVID-SEG are symbolized as "Combination". Utilizing CSSL, deprived of tuning up, through transfer learning, DenseNet 169 is pre-trained. Following explanations are made considering this table.

Firstly, including Lung masks can highly advance the working. By comparing the following:

- 'COVID-349 with Lungs mask only' and 'COVID-CT-349'.
- 'COVID-CT-118 with Lungs mask only' and '-COVID-CT-118'.
- 'Combination with Lungs mask only' and 'Combination'.

Compromising the AUC and precision, the integration Lungs mask considerably advances F1 on the COVID-SEG. Secondly, including the Lesion Masks can highly advance the working. It is obvious by comparing the following:

- 'COVID-SEG with Lesion mask only' and 'COVID-SEG'.
- 'Combination with Lesion mask only' and 'Combination'.

Thirdly, rather than utilizing only a lesion mask or only Lungs mask, utilize the two to get advanced results on mutual data set. Overall, the Lungs mask's practicality and Lesion mask can be determined by these outcomes, advancing diagnostic performance.

Table 6 Performance of test sets by using DenseNet-169 and

ResNet-50

| Train Data | Accuracy % | F1-score % | AUC % |
|---|---|---|---|
| COVID-CT-349 | 79.5 | 76.0 | 90.1 |
| COVID-CT-349 with lung mask only | 85.0 | 85.9 | 92.8 |
| COVID-Seg | 66.3 | 58.1 | 80.6 |
| COVID-Seg with lung mask only | 77.4 | 74.6 | 86.4 |
| COVID-Seg with lesion mask only | 60.4 | 42.6 | 74.1 |
| COVID-118 | 57.8 | 36.3 | 75.2 |
| COVID-118 with lung mask only | 73.3 | 66.4 | 86.2 |
| Combination | 74.5 | 70.1 | 89.8 |
| Combination with lung mask only | 86.2 | 87.2 | 97.6 |
| Combination with lesion mask only | 83.3 | 84.6 | 94.8 |
| Combination with lung and lesion masks | 89.0 | 90.1 | 98.0 |

The performance of DenseNet-169 training on the combined dataset is shown in Table 5. We made the given observations from this table; firstly, better performance is achieved by CSSL+TL achieves better as compared to TL (transfer learning). The effectiveness of CSSL demonstrates the improvement in learning representations. Secondly, transfer learning performs better compared to the random initialization. Using multi-task learning and leveraging CSSL pretraining by incorporating lung masks and lesion masks, the authors achieved an accuracy of 0.89 with an F1 of 0.90 and AUC of 0.98.

## 6. Conclusion

To substitute the expansion of AI-based approaches for consuming CT to screen and test the patients of COVID-19. The dataset comprises 349 CT images of COVID-19 of 216 patients and 463 CT images of COVID-19 negative patients used as negative test samples. A method has been established grounded on multi-task learning and contrastive self-supervised learning using these datasets. The experimental results attain 0.90 F1-score, 0.98 AUC, and 0.89 precision on the training sets of the health facilities' real CT images.

The main contribution of this study can be summarized in threefold; (1) We have proposed a diagnostic approach based on multi-task learning and self-supervised learning using three different CT datasets, (2) We compared the performance of two models, namely DenseNet-169 and ResNet-50 using three different techniques; lung mask, lesion mask and both combined, (3) We evaluated the models investigated in this work, and test their usability and accuracy on a sizeable combination generic dataset.

Future research on this issue should include examining automatic hyperparameter optimization approaches for self-supervised learning and transfer learning models and creating frameworks based on transfer learning that enable the processing of 3D CT images.

## Acknowledgment

The authors would like to acknowledge the support of Prince Sultan University for paying the Article Processing Charges (APC) of this publication.

## References

[1] HUANG L. Serial Quantitative Chest CT Assessment of COVID-19: A Deep Learning Approach. *Radiology: Cardiothoracic Imaging*, 2020, 2(2): e200075. doi: 10.1148/ryct.2020200075.

[2] LI L. Using Artificial Intelligence to Detect COVID-19 and Community-acquired Pneumonia Based on Pulmonary CT Evaluation of the Diagnostic Accuracy. *Radiology*, 2020, 296(2): E65–E71. doi: 10.1148/radiol.2020200905.

[3] XU X. Deep Learning System to Screen Coronavirus Disease. *Pneumonia*, 2019, 29.

[4] ZHENG C. Deep Learning-based Detection for COVID-19 from Chest CT using Weak Label. *Infectious Diseases (except HIV/AIDS)*, 2020. doi: 10.1101/2020.03.12.20027185.

[5] GOZES O. Rapid ai development cycle for the coronavirus (COVID-19) pandemic: Initial results for automated detection and patient monitoring using deep learning ct image analysis.

[6] YING S. Deep learning Enables Accurate Diagnosis of Novel Coronavirus (COVID-19) with CT images. *Radiology and Imaging*, 2020. doi: 10.1101/2020.02.23.20026930.

[7] SHI F. Large-Scale Screening of COVID-19 from Community-Acquired Pneumonia using Infection Size-Aware Classification. No date, 8.

[9] COHEN JP, MORRISON P, DAO L. COVID-19 Image Data Collection. *arXiv:2003.11597 [cs, eess, q-bio]*, 2020. http://arxiv.org/abs/2003.11597.

[10] CHOWDHURY MEH. Can AI Help in Screening Viral and COVID-19 Pneumonia? *IEEE Access*, 2020, 8: 132665–132676. doi: 10.1109/ACCESS.2020.3010287.

[11] HUANG G, LIU Z, VAN DER MAATEN L, WEINBERGER KQ. Densely Connected Convolutional Networks. *2017 IEEE Conference on Computer Vision and Pattern Recognition (CVPR)*, 2017, 2261–2269. doi: 10.1109/CVPR.2017.243.

[12] HE K, ZHANG X, REN S, SUN J. Deep Residual Learning for Image Recognition. *arXiv:1512.03385 [cs]*, 2015. http://arxiv.org/abs/1512.03385.

[13] DENG J, DONG W, SOCHER R, LI L-J, LI K, FEI-FEI L. ImageNet: A Large-Scale Hierarchical Image Database. No date, 8.

[14] KINGMA DP, BA J. Adam: A Method for Stochastic Optimization. *arXiv:1412.6980 [cs]*, 2017. http://arxiv.org/abs/1412.6980.

[15] NASEER S, ALI RF, MUNEER A, FATI SM. IAmideV-deep: Valine amidation site prediction in proteins using deep learning and pseudo amino acid compositions. *Symmetry*, 2021, 13(4): 560.

[16] MUNEER A, FATI SM, FUDDAH S. Smart health monitoring system using IoT based smart fitness mirror. *Telkomnika*, 2020, 18(1): 317-331.

[17] NASEER S, ALI RF, FATI SM, MUNEER A. iNitroY-Deep: Computational Identification of Nitrotyrosine Sites to Supplement Carcinogenesis Studies Using Deep Learning. *IEEE Access*, 2021, 9: 73624-73640.
[18] FATI SM, MUNEER A, AKBAR NA, TAIB SM. A Continuous Cuffless Blood Pressure Estimation Using Tree-Based Pipeline Optimization Tool. *Symmetry*, 2021, 13(4): 686.
[19] LAWTON S, VIRIRI S. Detection of COVID-19 from CT Lung Scans Using Transfer Learning. *Computational Intelligence and Neuroscience*, 2021.
[20] JUN M., CHENG G., YIXIN W., XINGLE A., JIANTAO G., ZIQI Y., MINQING Z., XIN L., XUEYUAN D., SHUCHENG C., HAO W., SEN M., XIAOYU Y., ZIWEI N., CHEN L., LU T., YUNTAO Z., QIONGJIE Z., GUOQIANG D., and JIAN H. COVID-19 CT Lung and Infection Segmentation Dataset (Verson 1.0) [Data set]. Zenodo, 2020. https://doi.org/10.5281/zenodo.3757476
[21] MEDICAL SEGMENTATION. *COVID-19 CT segmentation dataset*, 2020. http://medicalsegmentation.com/covid19/

**参考文:**

[1] HUANG L. 新冠肺炎的連續定量胸部 計算機斷層掃描 評估：一種深度學習方法。放射學：心胸成像，2020 年，2(2)：e200075。土井：10.1148/ryct.2020200075。
[2] LI L. 基於肺 計算機斷層掃描 診斷準確性評估，使用人工智能檢測 新冠肺炎和社區獲得性肺炎。放射學，2020 年，296(2)：E65-E71。土井：10.1148/radiol.2020200905。
[3] XU X. 篩查冠狀病毒疾病的深度學習系統。肺炎，2019，29。
[4] ZHENG C. 使用弱標籤從胸部 計算機斷層掃描 進行基於深度學習的 新冠肺炎檢測。傳染病（艾滋病毒/艾滋病除外），2020 年。土井：10.1101/2020.03.12.20027185。
[5] GOZES O. 冠狀病毒 (新冠肺炎) 大流行的快速人工智能開發週期：使用深度學習 ct 圖像分析進行自動檢測和患者監測的初步結果。
[6] YING S. 深度學習利用 計算機斷層掃描 圖像準確診斷新型冠狀病毒 (新冠肺炎)。放射學和影像學，2020。土井：10.1101/2020.02.23.20026930。
[7] SHI F. 使用感染大小感知分類從社區獲得性肺炎中大規模篩查 新冠肺炎。沒有日期，8。
[9] COHEN JP、MORRISON P、DAO L. 新冠肺炎圖像數據收集。arXiv:2003.11597 [cs, 埃斯, q-生物], 2020. http://arxiv.org/abs/2003.11597。
[10] 喬杜里·梅。人工智能能否幫助篩查病毒性和 新冠肺炎肺炎？IEEE 訪問，2020 年，第 8 期：132665–132676。土井：10.1109/ACCESS.2020.3010287。
[11] HUANG G, LIU Z, VAN DER MAATEN L, WEINBERGER KQ. 密集連接的捲積網絡。2017 IEEE 計算機視覺和模式識別會議，2017，2261–2269。土井：10.1109/CVPR.2017.243。
[12] HE K, ZHANG X, REN S, SUN J. 圖像識別的深度殘差學習。arXiv：1512.03385 [cs]，2015 年。http://arxiv.org/abs/1512.03385。
[13] DENG J, DONG W, SOCHER R, LI L-J, LI K, FEI-FEI L. 圖像網：大規模分層圖像數據庫。沒有日期，8。
[14] KINGMA DP，BA J. 亞當：隨機優化方法。arXiv：1412.6980 [cs]，2017 年。http://arxiv.org/abs/1412.6980。
[15] NASEER S、ALI RF、MUNEER A、FATI SM。一世一種米德伏——深的：使用深度學習和偽氨基酸組成預測蛋白質中的纈氨酸酰胺化位點。對稱性，2021 年，13（4）：560。
[16] MUNEER A、FATI SM、FUDDAH S. 使用基於物聯網的智能健身鏡的智能健康監測系統。 電信，2020, 18(1): 317-331。
[17] NASEER S、ALI RF、FATI SM、MUNEER A. 一世硝基是深的：使用深度學習補充致癌研究的硝基酪氨酸位點的計算識別。 電子電氣設備訪問，2021，9：73624-73640。
[18] FATI SM、MUNEER A、AKBAR NA、TAIB SM。使用基於樹的管道優化工具進行連續無袖帶血壓估計。對稱性，2021 年，13（4）：686。
[19] LAWTON S, VIRIRI S. 使用遷移學習從 計算機斷層掃描 肺掃描中檢測 新冠肺炎。計算智能和神經科學，2021 年。
[20] JUN M., CHENG G., YIXIN W., XINGLE A., JIANTAO G., ZIQI Y., MINQING Z., XIN L., XUEYUAN D., SHUCHENG C., HAO W., SEN M. , XIAOYU Y., ZIWEI N., CHEN L., LU T., YUNTAO Z., QIONGJIE Z., GUOQIANG D., 和 JIAN H. 新冠肺炎计算机断层扫描肺和感染分割数据集（版本 1.0）[数据集]．芝诺多，2020 年。https://doi.org/10.5281/zenodo.3757476
[21] 医学分割。新冠肺炎计算机断层扫描 分割数据集，2020。http://medicalsegmentation.com/covid19/